Pharmaceutical Research, Vol. 27, No. 3, March 2010 (© 2010)
DOI: 10.1007/s11095-009-0025-x

Research Paper

A Semi-physiological-Based Pharmacokinetic/Pharmacodynamic Model to Describe the Effects of Topotecan on B-Lymphocyte Lineage Cells

Nieves Vélez de Mendizábal,[1,2] Iván Martínez-Forero,[3,4] María J. Garrido,[5] Eva Bandrés,[6] Jesús García-Foncillas,[6] Cristina Segura,[5] and Iñaki F. Trocóniz[5,7]

Received August 6, 2009; accepted December 3, 2009; published online January 26, 2010

Purpose. To develop a semi-physiological-based model describing simultaneously the time course of immature and mature B-lymphocytes after topotecan (TPT) administration to tumor-bearing rats.
Methods. Twenty-four tumor-bearing BDIX male rats received a single 6 mg/kg intra-peritoneal dose of TPT or saline. Mature and immature B-cell levels were measured every two days during three weeks and showed a very different temporal pattern. Both B-cell populations
declined rapidly, reaching the nadir at 3–4 days after TPT administration; however, mature cells returned to baseline at day 8, while immature B-cells stayed at nadir until day 9 instead. Data were modeled using the population approach with NONMEM VI.
Results. The model developed maintains the proliferation, maturation and degradation elements of previous published models for myelosuppresion. In order to describe the rapid recovery of mature cells, it includes a peripheral compartment providing a constant supply of mature cells to the bloodstream.
Conclusions. The major contribution of the model is its new structure and the dynamical consequences, demonstrating an independent behavior between mature and immature B-cells during recovery. The final model could represent a good basis for the optimization of cytotoxic drugs oriented to attain a maximum antitumor efficacy while minimizing hematological toxicity.

KEY WORDS: B-lymphocytes; homeostasis; pharmacokinetic-pharmacodynamic model; Topotecan.

INTRODUCTION

Chemotherapy complications are common among cancer patients. Cytotoxic drugs impair cell renewal in tissues with high reproduction rate, such as the gastrointestinal and the hematopoetic systems. One of the most prevalent side effects derived from chemotherapy is the hematological toxicity, reflected as leukopenia. Myelosupression is the most common dose-limiting toxicity during a chemotherapy regimen and may compromise treatment efficacy. In this regard, it is of major clinical interest to understand which are the determinants for leukopenia development in order to optimize dosing strategies and predict the appearance of infectious complications (1,2).

Pharmacokinetic/pharmacodynamic (PK/PD) modeling is well-suited to address that need (3). During the last years, semi-mechanistic models for myelosupression have been used to describe the hematological effects of different cytotoxic agents already in clinical use or during development (4–9). However, the question regarding whether the mechanism of drug action and the complex process of blood cells production and homeostasis are completely captured is still open. The answer is of importance if, for example, one is interested in predicting the time course of leukopenia on the basis of biological parameters previously reported and on *in vivo* drug-related experimental data. It is also relevant if we are willing to design a new dose regimen based on the results of the PK/PD model. In the case of leukopenia, PK/PD modeling could be used to guide the decision of whether or not to implement rescue treatment in the way of GM-CSF (10,11).

PK/PD models for myelosupression usually consider compartments resembling blood cell maturation processes (4,5). The readout of these models is mature cell number, ignoring the immature population and taking as granted that the dynamic behavior of mature cells follows the one of immature cells. For example, Fig. 1A shows the general form of the model developed by Friberg *et al.* (4) and the simulated time course on each of the cell compartments. As we can see, the dynamic behavior of mature cells follows the one of immature cells, and the dynamic

Electronic supplementary material The online version of this article (doi:10.1007/s11095-009-0025-x) contains supplementary material, which is available to authorized users.

[1] Neuroimmunology Laboratory, Center for Applied Medical Research, University of Navarra, Pamplona, Spain.
[2] Department of Computational Sciences and Artificial Intelligence, University of the Basque Country, San Sebastian, Spain.
[3] Gene Therapy Unit, Center for Applied Medical Research, University of Navarra, Pamplona, Spain.
[4] Department of Physics and Applied Mathematics, University of Navarra, Pamplona, Spain.
[5] Department of Pharmacy and Pharmaceutical Technology, School of Pharmacy, University of Navarra, Pamplona 31080, Spain.
[6] Laboratory of Pharmacogenomics, Cancer Research Program (Center for Applied Medical Research), University of Navarra, Pamplona, Spain.
[7] To whom correspondence should be addressed. (e-mail: itroconiz@unav.es)

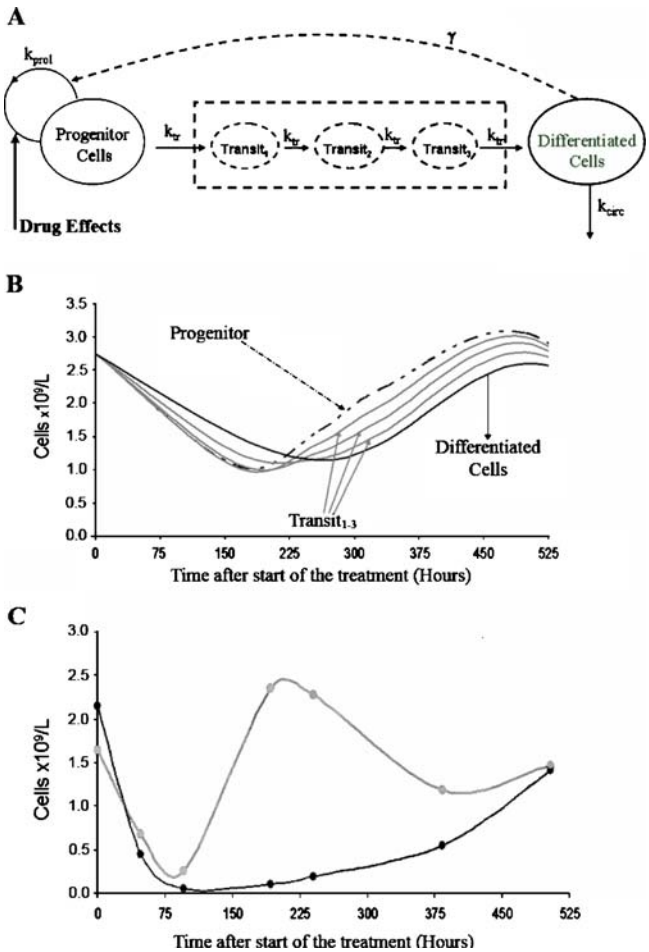

Fig. 1. A. Semi-mechanistic model of neutropenia proposed by Friberg *et al.* (13); **B.** Simulated time course in each of the five different compartments of the model after a single administration of a cytotoxic drug; **C.** Immature (*black*) and mature (*grey*) B-cells observed profiles in one of the animals treated with TPT at the dose of 6 mg/kg administered intra-peritoneal.

of immature population follows the behavior of the progenitor cells (Fig. 1B). However, there is experimental evidence indicating that this kind of dynamic does not correspond to reality, at least for the case of the B-cell lineage (12).

In fact, the lymphopenia caused by topotecan (TPT) administered to tumor-bearing rats led us to observe a cellular population dynamic as complex as the one shown in Fig. 1C, which could not be described with the previous published model applied to myelosuppression. Thus, the discrepancy between time profiles experimentally observed and those simulated using previous PK/PD models for myelosuppression justifies the endeavor of developing a new model.

B-cells are produced in the bone marrow. Early differentiation occurs through a well-described mechanism of intermediate subpopulations (pro-b, pre-b-lymphocytes). B-cell maturation takes place in secondary lymphoid organs such as the spleen (13). Mature B-cells continually travel across the body searching for their cognate antigen (14). Migration is controlled by chemokines secreted in response to danger signals.

Although, the specific effect over lymphoid lineage cells is not the most limiting factor in chemotherapy, the immune system plays a fundamental role in the antitumor mechanisms of action of conventional chemotherapy drugs including cytotoxic agents. In particular, chemotherapy can promote immunogenic cell death and release tumor antigens capable of activating T- and B-cells (15,16). In the same way, cytotoxic drugs can deplete tolerogenic immune cells that prevent lymphocytes to mount a successful response against the tumor.

Therefore, the main objective of this work is the development of a new semi-mechanistic PK/PD model capable of accurately and simultaneously describing the evolution of immature and mature B-cells after TPT administration, taking into account that lymphoid cells are involved in the toxicity and efficacy effects.

Mature B-lymphocytes derive from immature precursors. Immature B-cells can proliferate in response to new antigens, while mature lymphocytes get involved in the defense agains, previously encountered challenges. Therefore, in the case of cytotoxic agents (i.e TPT) immature B-cell measurement could serve as an indicator of susceptibility to infectious complications. This phenomenon has already been reported in patients after rituximab treatment that are more prone to acquire influenza infections (17).

MATERIALS AND METHODS

The data presented and analyzed in the current work were obtained from a study previously published (18) in which the pharmacokinetics of TPT and the time course of neutrophils, leucocytes, and total (immature and mature) B-lymphocytes were modelled.

Animals and Tumour Implantation

Twenty-four males BDIX rats (CRIFFA, Barcelona, Spain) weighing 300±25 g were housed in microisolator cages under positive-pressure ventilation and maintained in closed-shelf, laminar-flow racks to avoid contact with pathogens, odors or noises and kept under standard laboratory conditions. Sterilized food and water were available *ad libitum*. To induce the tumor, 250 μL of PBS containing $1x10^6$ DHD/K12PROb cells (syngenic adenocarcinoma cell line of BDIX rats) were subcutaneously injected into the right side of the chest.

The protocol of the study was approved by the Animal Experimentation Committee of the University of Navarra and is in accordance with the applicable European guidelines.

Experimental Design and Haematological Response

Three weeks after cells inoculation, animals were randomly divided into two groups: Group I (control group, n=11) received an i.p. physiological saline (pH 3) solution, and group II (treated group, n = 13) was administered i.p. with 6 mg/kg of TPT (prepared in saline pH 3).

To measure the haematological response, several blood samples were collected at different times during the experiment: before saline or TPT administration, corresponding to baseline value of each animal, and every three or four days during three weeks. Blood (250 μL) samples were collected in EDTA-prepared tubes from the retro-orbital sinus with the

animal lightly anesthetized. All samples were always collected between 9 and 10 a.m. and immediately processed. Phenotypic analysis of lymphocyte subpopulations in peripheral blood samples was carried out according to the follow scheme (19):

(i) An aliquot of each sample was used to determine the total leukocyte counts by a Coulter MicroDiff II Analyser (Coulter Corp., Hialeah, FL, USA) within 3 h of blood extraction.
(ii) The analysis of lymphocyte subsets was evaluated by a flow cytometer (Becton-Dickinson, San Jose, CA, USA) assay. The antibodies used to evaluate the lymphocyte populations were CD90 to distinguish between lymphocytes mature (CD90-) and immature (CD90+), CD45 (for lymphocytes B), CD8 and CD4 (for lymphocytes T) and NK expression.

Briefly, 100 μl of whole blood was added to tubes containing 10 μl of R-Phycoerytrin(R-PE)-conjugated mouse anti-rat CD90 (Thy-1) monoclonal antibody (Becton-Dickinson) and 10 μl of R-Phycoerytrin(R-PE)-conjugated mouse anti-rat CD45RA (OX-33), anti-CD8 (OX8), anti-CD4 (W3/25) monoclonal antibody (Becton-Dickinson) and incubated for 15 min. Following incubation, red cells were lysed using FACS Lysing Solution, and the expression for the surface markers of different antigens was analysed gating the region of lymphocytes. Labelled cells with isotype-matched irrelevant monoclonal antibody were included as a control. Absolute B- or T-lymphocyte counts were calculated on the basis of total leukocyte number. Mature B-cells were estimated by subtracting the number of CD90-CD45+ cells from total B-cells identified by means of CD45RA antibody. The same procedure was followed to estimate and quantify the mature T-cells (CD90- CD4+; CD90- CD8+). With this procedure mature (CD90- CD45+) and immature (CD90+ CD45+) B-cells could be separated and quantified for a posterior analysis (20).

DATA ANALYSIS

The population approach using the First Order Conditional Estimation method with the INTERACTION option implemented in the software NONMEM, version VI (21) was used to estimate the parameters of the potential model candidates.

Inter-animal variability (IAV) was modelled exponentially as $p_i = p_{pop} \times e^{\eta_p}$, where p_{pop} represents the typical estimate of the parameter p in the population, p_i corresponds to the value of the p parameter in the i^{th} individual, and η_p represents a random variable symmetrically distributed around 0 with variance of ω^2, and corresponding to the deviation between the individual parameter value and the typical population estimate.

Residual variability was initially described with a combined error model of the form: $Obs_{i,j} = Pred_{i,j} \times (1+\varepsilon_{ij,1}) + \varepsilon_{ij,2}$, where $Obs_{i,j}$ represents the observation (immature or mature cells) in the i^{th} individual at time j^{th}, and $Pred_{i,j}$ is the corresponding model predicted value. The concentration proportional and additive parts of the combined error model are represented by $(1+\varepsilon_{ij,1})$ and $\varepsilon_{ij,2}$, respectively, and both account for the deviation between the predicted and observed values. ε_1, ε_2, are random variables symmetrically distributed around 0 with variance of σ_1^2 and σ_2^2, respectively.

Selection between models was based on the precision of parameter estimates, goodness-of-fit plots, and the minimum value of objective function [-2 log(likelihood); –2LL] provided by NONMEM. For two nested models, a decrease in 3.84, or 6.63, points in -2LL for an extra parameter was considered significant at the 5 or 1% level, respectively. In the case of models that were not nested, –2LL was not used directly for comparative purposes, and the value of the Akaike Information Criteria (AIC) (22) computed as $-2LL + 2 \times Np$, where Np is the number of the parameters in the model, was used instead. In those cases, the model with the lowest value of AIC, given that precision of model parameters and data description were adequate, was selected.

The selected model was evaluated thorough the predictive (visual and numerical) checks (23).

Visual predictive check: For each type of cell (immature and mature) and for each treatment condition (control and treated), one-thousand cell *-vs.-* time profiles were generated based on the selected model and its parameter estimates. At each experimental time, the 2.5, 50, and 97.5th percentiles were then calculated, and the agreement between simulations and raw data was inspected visually.

Numerical predictive check: One thousand datasets with the same design characteristics as the original study were simulated. The median value at nadir and the median time to achieve the nadir were computed in each dataset for the case of the immature and mature cells. Then, the 2.5, 50, and 97.5th percentiles of the distribution of the two data descriptors (nadir and time to nadir) were calculated from the 1,000 simulated datasets and compared with the corresponding median values obtained from the raw data.

Graphical representations and generation of simulation results were done with the S-PLUS 6.2. Professional Edition (Copyright 1988, 2002 Insightful Corp.) software.

Model Description

Pharmacokinetic Model

Drug effects are incorporated in the model (see below) as a function of the plasma concentration levels of TPT predicted by the pharmacokinetic model (C_P). Pharmacokinetics of TPT in BDIX rats after i.p. administration of a 6 mg/kg dose have been already reported (18). A two-compartmental disposition model with a first-order absorption was used to describe the time course of the observed levels of TPT in plasma. The three ordinary differential equations (ODEs) corresponding to the pharmacokinetic model used in the current analysis are

$$\frac{dA_{ip}}{dt} = -K_A \times A_{ip}$$

$$\frac{dA_P}{dt} = K_A \times A_{ip} + \left(\frac{CL_D}{V_T}\right) \times A_T - \left(\frac{CL_D + CL}{V}\right) \times A_P$$

$$\frac{dA_T}{dt} = \left(\frac{CL_D}{V_T}\right) \times A_P - \left(\frac{CL_D}{V}\right) \times A_T$$

where $dA_{ip,P,T}/dt$ represents the rate of change in the intraperitoneal, central (plasma), and tissue (peripheral) compart-

ments, respectively; K_A is the first-order rate constant of absorption; CL is the total plasma clearance; CL_D is the intercompartmental clearance; and V and V_T are the apparent volumes of distribution of the central and peripheral compartments, respectively. C_P is calculated as A_P/V. The estimates of K_A, CL_D, CL, V and V_T used in the analysis were 20.1 day^{-1}, 0.58 $L\times day^{-1}$, 1.32 $L\times day^{-1}$, 1.44 L, and 2.36 L, respectively. The magnitude of IAV (expressed as coefficient of variation) for K_A was 32% (18). At time 0 (initial condition) A_{ip}=Dose (6 mg/kg), A_P and A_T=0.

Physiological-Based Model for B Lymphocyte Lineage Cells

Different models were fit to the immature and mature cell data and discussed in the "Results" section. The main focus of this model-building stage was to develop a model that adequately describes the observations with precise estimation of parameters. Initial parameter estimates for the different models explored were approximated using the System Dynamics (SD) framework that combines the power of differential equations with a graphical design and representation of the variables. The models were simulated in the VENSIM (Ventana Systems, Inc., MA, United States.) and MATLAB (The Mathworks, MA, United States) computing environments.

The final selected model that appears schematically represented in Fig. 2 and consists of the following system of ODEs:

$$\frac{dProl}{dt} = k_{prol} \times D_{Effect} \times Prol \times \left[\frac{Prol_0}{Prol_t}\right]^{\gamma_1} - k_{tr} \times Prol$$

$$\frac{dImm}{dt} = k_{tr} \times Prol - k_{tr} \times (1 + \theta_{SLP} \times t) \times Imm$$

$$\frac{dMat}{dt} = k_{tr} \times (1 + \theta_{SLP} \times t) \times Imm + k_{pool} \times Delayed_3 - k_{circ} \times Mat$$

$$D_{Effect} = 1 - \theta_{Drug} \times C_P$$

$$\frac{dDelayed_1}{dt} = k_{del} \times \left[\frac{Mat_0}{Mat_t}\right]^{\gamma_2} - k_{del} \times Delayed_1$$

$$\frac{dDelayed_2}{dt} = k_{del} \times Delayed_1 - k_{del} \times Delayed_2$$

$$\frac{dDelayed_3}{dt} = k_{del} \times Delayed_2 - k_{del} \times Delayed_3$$

where, dX/dt represents the rate of change in the corresponding compartment [proliferative cells (Prol); immature cells (Imm), mature cells (Mat), and Delayed]; k_{prol}, k_{tr}, and k_{circ}, are the first-order rate constants of proliferation, maturation, and degradation, respectively. D_{Effect}, accounts for the lymphocyte effects of TPT, where θ_{Drug} reflects the magnitude of such effects. The parameter θ_{SLP} allows for describing the decrease in the immature cells observed in the control group. This effect could be explained by tumour inoculation and physical stress. The continuous supply of matured cells into the bloodstream from a peripheral compartment (i.e., spleen) is represented by $k_{Pool}\times Delayed_3$, where k_{pool} is a zero-order rate constant (assuming that the amount of cells in the peripheral compartment remains constant regardless of the perturbations occurring in the differentiated cells and delayed compartments), and $Delayed_3$, the magnitude of a

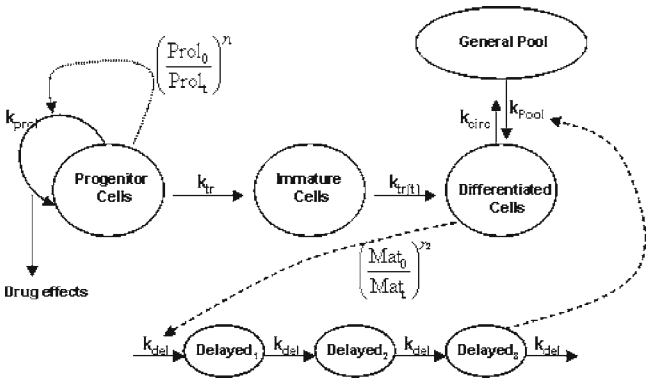

Fig. 2. Schematic representation of the model selected to describe simultaneously the time course of the immature and mature B-lymphocytes after a single administration of TPT. Parameters are defined in the text.

signal that affects k_{pool}. This delay represents the time required for cytokines, produced or stimulated by B-cells, to promote B-cell homeostasis. This process needs a signal transduction delay associated, for example, with novo gene expression (24).

The model incorporates two feedback mechanisms governed by γ_1 and γ_2, and the drug-induced change in proliferative and mature cells with respect to the corresponding levels at baseline $Prol_0$ and Mat_0, respectively. The feedback mechanism represented by $(Prol_0/Prol_t)^{\gamma 1}$ has an instantaneous effect on k_{prol}.

On the other hand, the decrease of mature cells with respect to Mat_0 induces a non-instantaneous increase in the lymphocyte supply. This delay is governed by the first-order rate constant k_{del}. The initial conditions of the system are given by the following expressions:

$$k_{tr} = k_{prol}$$

$$k_{pool} = k_{circ} \times Mat_0 - k_{tr} \times Imm_0$$

$$Prol_0 = Imm_0$$

$Mat_0=\theta_{Frc}\times Imm_0$ [θ_{Frc}, represents the ratio (different from 1) between Mat_0 and Imm_0, the baseline levels of immature cells].

$$Delayed_{1,0} = Delayed_{2,0} = Delayed_{3,0} = 1.$$

MODEL EXPLORATION

After developing a complex model as the one selected in the current work, it is often desirable to explore its behaviour varying the degree of perturbation. Hence, we have explored the behaviour of the model simulating 1,000 time profiles of immature and mature cells corresponding to different i.p. doses of TPT uniformly distributed and ranging between 0 and 6 mg/kg. Simulations were based on the typical parameter estimates of the selected physiological model. It should be taken into account that it is not possible to ensure that model predictions at those dose/regimen scenarios would

describe data obtained under those experimental settings. The aim of the simulation exercise was to explore the dynamic properties of the model under different degrees of perturbations.

Two types of TPT administration schedules were simulated. The first one corresponded to a single TPT i.p. dose (schedule A), and the second consisted of five doses administered once daily (schedule B). The total TPT dose administered in both schedules was the same.

Three types of descriptors were explored during that simulation exercise: (i) time course of immature and mature B-cells, (ii) contribution of the continuous supply of mature B-cells represented by k_{Pool}, and (iii) the maximum percentage of toxicity calculated as $100\times[1-(\text{nadir/baseline})]$.

RESULTS

Fig. 1C shows the time profiles of immature and mature B-lymphocytes after a single i.p. 6 mg/kg dose of TPT in one rat chosen at random (for clarity). After drug administration, the two populations followed a very different dynamic pattern. Meanwhile, both type of B-cells declined rapidly, reaching the nadir at 3–4 days; mature cells returned to baseline levels at day 8. However, immature B-cells stayed at low levels until day 9 and recovered baseline levels after three weeks. The rebound phenomena occurring for the mature cells is also very clear. Those dynamic patterns are consistent in all animals treated with TPT, as it can be seen in the observations displayed in Fig. 3.

Model Development

A total of 468 B-cell samples [mature: 234; immature: 234] were used to develop the selected model, which maintains the proliferation, maturation and degradation elements of previous published models (4,5). Drug effects were incorporated on the first-order rate of proliferation as it has been shown previously (4) and in accordance with the known mechanism of hematological toxicity of anticancer drugs.

The rapid recovery of mature cells, in part independently of immature cells, led us to include a new compartment for peripheral mature B-cells. Such compartment provides a constant supply of mature cells to the bloodstream at a constant rate given by the estimate of k_{pool}. However, after a perturbation (i.e. TPT administration) strong enough to reach a threshold in circulating B-cells, the pool increases the release of mature B-cells to the bloodstream, allowing them to return to the basal state previous to the perturbation. The biological significance of the compartment has been reported previously in mice, where the size of the peripheral B-cell pool is not determined by the number of bone marrow precursors, but instead of the available resources in terms of cytokines or growth factors (25).

Table I lists the results of –2LL and AIC for the main models fit to the immature and mature cell data.

The rebound observed in the profiles of mature cells was captured by incorporating a delay in the signal originated by the decrease on mature cells in respect to baseline, through a series of transit compartments. Alternative models where the maturation rate increased as a function of the decrease in the immature or proliferation cells were also considered, but they resulted in worse fits (see models 2 and 3 in Table I).

The well-established model for neutropenia (4) shows a feedback mechanism on the rate of proliferation triggered by the decrease in the circulating mature cells with respect to baseline. However, in the current analysis, the best description of the data was obtained when the feedback was included between proliferating cells and their own rate of proliferation. Models 4 and 5 in Table I correspond to the models where the feedback on the proliferation rate was controlled by the immature or mature cells, respectively, and the resulted –2LL and AIC values were clearly higher than the selected model (model 1 in Table I). Models 6 and 7 in Table I indicate that both feedback mechanisms were required to describe the data ($P<0.01$).

Adding an extra transit compartment between the progenitor and the immature compartments did not improve the fit. The same result was found when the transit compartment was located between the immature and mature cells compartments (models not shown).

When an E_{MAX} or a sigmoidal E_{MAX} model was used to describe drugs effects (model 8 and in Table I), parameters of the drug effect model were highly correlated, and the –2LL values remained almost unchanged in respect to the selected model.

The decrease in the immature cells observed in the control group, and shown in the upper left panel of Fig. 4, could be described increasing k_{tr} linearly as a function of time ($P<0.01$)

Lastly, an extra elimination process from the immature cells compartment was incorporated in the model, but the fit did not improve ($P>0.05$).

IAV was tested in all model parameters but gave significant results only for the parameters $Immt_0$ and γ_2 ($P<0.01$). However, confidence interval for the two IAV terms included the zero value. When the log-likelihood profiling method was used to explore in more detail the confidence intervals, it was found that the confidence interval of IAV on γ_2 included the zero value again, but not in the case of the IAV for $Immt_0$.

Residual variability in the case of the immature cells was described with a combined error model. An additive model was used in the case of the mature cells.

During the modeling exercise transformation, both sides (i.e., logarithmic and box-cox) were also considered, but they did not provide any benefit to model performance compared to the linear scale.

Table II lists the population model parameter estimates corresponding to the selected model. It is worth noting that most of the parameters were estimated with high precision as it is reflected by their coefficients of variation that are lower than 20%. The confidence interval expressed in CV(%) for IAV in γ_2 calculated using the log-likelihood profiling method, was 5.5–18%.

Individual model-predicted profiles for immature and mature cells are shown in Fig. 3, and for all the animals studied, the model describes the individual data very well. η-, and ε-shrinkage (26) show values of 19 and 2.1% (immature cells) and 2% (mature cells), respectively, indicating that goodness-of-fit plots and the individual predictions shown in Fig. 3 are reliable

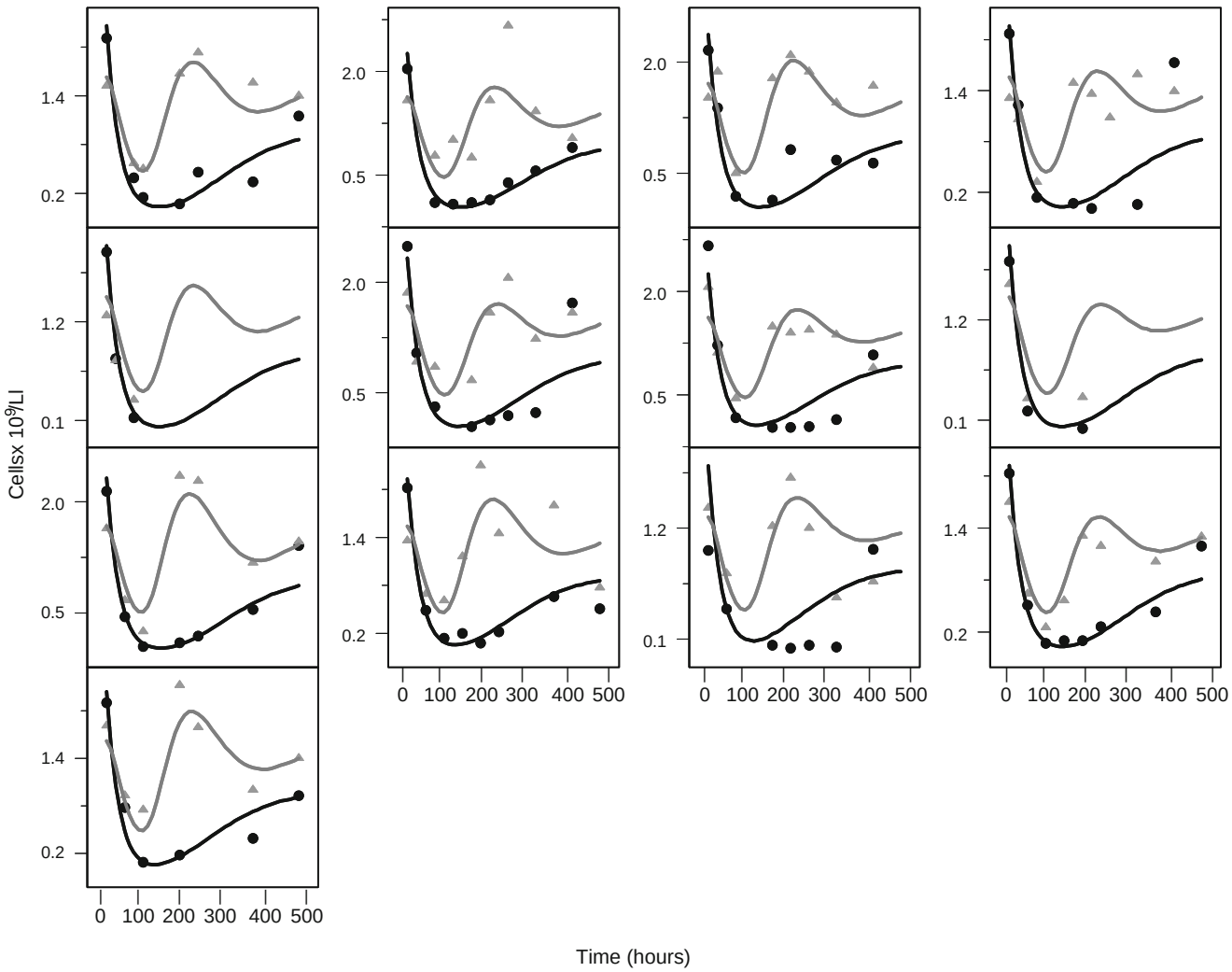

Fig. 3. Individual model predicted (*solid lines*) and observed (*points*) time profiles of immature (*black*) and mature (*grey*) B lymphocytes. Each panel represents a single animal treated with TPT.

Fig. 4 shows the results obtained from the visual predictive check where it can be observed that, for the two groups of animals (control and treated) and the two types of measurements (immature and mature), the model captures very well the mean tendency of the data and their dispersion. The results obtained from the numerical predictive check indicated also that the model was supported by the data. For the case of the immature cells, the median values of nadir and

Table I. List of Main Model Fit to the Immature and Mature Cells Data After Administration of TPT

Model	Changes in model structure with respect to the selected model (Fig. 2)	−2LL	AIC	Δ-2LL/AIC
1	None	−365.849	−339.849	–
2	$k_{prol} \times \left[\frac{Immt_0}{Imm_t}\right]^{\gamma_1}$	−291.475	−265.475	+74.374
3	$k_{prol} \times \left[\frac{Mat_0}{Mat_t}\right]^{\gamma_1}$	−356.158	−330.158	+9.691
4	$k_{del} \times \left[\frac{Immt_0}{Imm_t}\right]^{\gamma_1}$	−122.739	−96.739	+243.11
5	$k_{del} \times \left[\frac{Prol_0}{Prol_t}\right]^{\gamma_1}$	−327.935	−301.935	+37.914
6	$\gamma_1 = 0$	−224.387	−200.837	+141.462
7	$\gamma_2 = 0$	−263.301	−239.301	+102.548
8	$D_{Effect} = 1 - \frac{E_{MAX} \times C_P^{\gamma}}{C_{50}^{\gamma} \times C_P^{\gamma}}$	−366.142	−336.142	−0.293

–2LL -2 log(likelihood), *AIC* Akaike Information Criteria, *Δ-2LL/AIC* changes in –2LL and AIC with respect to the selected model (Fig. 2), respectively

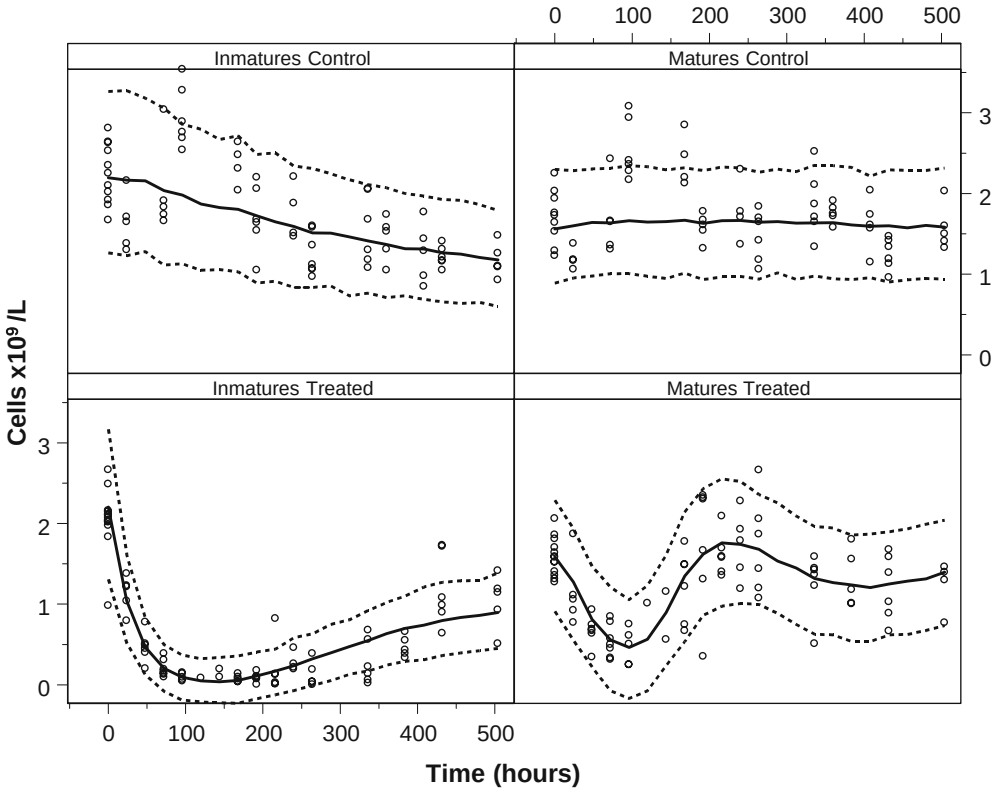

Fig. 4. Results from the visual predictive check. Points, observations. Lines, correspond to the 50th (*solid*) and 2.5th and 97.5th (*dashed*) percentiles obtained from 1,000 thousand simulations corresponding to an intra-peritoneal dose of TPT of 0 (control) and 6 mg/kg (treated).

time to nadir calculated from the raw data (0.06 cells$\times 10^9$/L and 161 h, respectively) were well-described by the simulations [median (2.5th–97.5th percentiles)]: 0.025 [0.0013–0.08] cells$\times 10^9$/L, and 153 [127–183]h, respectively. The results for the mature cells are 0.47 cells$\times 10^9$/L and 96 h, (raw data), and 0.45 [0.25–0.63] cells$\times 10^9$/L and 101 [66–160] h (model simulations).

Table II. Model Parameter Estimates Corresponding to the Selected Model

Parameter	Estimate	CV(%)
$Immt_0$ (cell$\times 10^9$/L)	2.22	4.6
θ_{Frc} (−)	0.72	3.5
k_{circ} (h^{-1})	0.049	7.9
k_{prol} (h^{-1})	0.031	4.8
k_{del} (h^{-1})	0.021	6.1
γ_1	0.205	13.6
γ_2	2.63	6.9
θ_{drug} (mL$\times$ng^{-1})	0.141	13.6
θ_{SLP} (h^{-1})	0.0018	11.6
IAV_{Inmt0} (%)	10	60
Residual $error_{Immt}$ (%)	25	34
Residual $error_{Immt}$ (cell$\times 10^9$/L)	0.17	61
Residual $error_{Mat}$ (cell$\times 10^9$/L)	0.39	13.9

Precision of parameter estimates is represented by the corresponding coefficient of variation [CV(%)] calculated as the ratio between the standard error provided by NONMEN and the estimate of the parameter, and multiplied by 100. Inter-animal variability (IAV) and residual variability are expressed as CV(%). Model parameters are defined in the text.

MODEL EXPLORATION

The model behaviour was explored varying uniformly the dose of TPT within the range from 0 to 6 mg/kg under two different dosage designs. In the case of immature cells, TPT produces a delayed loss (compared to the drug profiles in plasma), since it is the decline in the progenitor population which makes immature population decrease (Fig. 5A). Fig. 5B shows the loss and rapid recovery of the mature cells after the administration of different TPT doses. Although it is evident that mature cells are influenced by the immature cells, i.e. the loss of mature cells is produced by the loss of immature cells, there is another input flow of new mature cells, which does not depend on the immature population. Such input, controlled by a non-linear positive feedback, allows a fast return to homeostatic levels of mature B-cells. The recovery is able to produce a rebound effect. That is, after the loss of mature population, mature B-cells transiently reach values over the normal count. This effect is mainly due to the information delay in the feedback that controls the input of new cells from the pool, and is proportional to the loss of mature B cells.

Fig. 6 shows the time needed to recover 70, 80 and 85% of the basal value for mature cells depending on the total dose of TPT. Note that the time to recovery was longer for

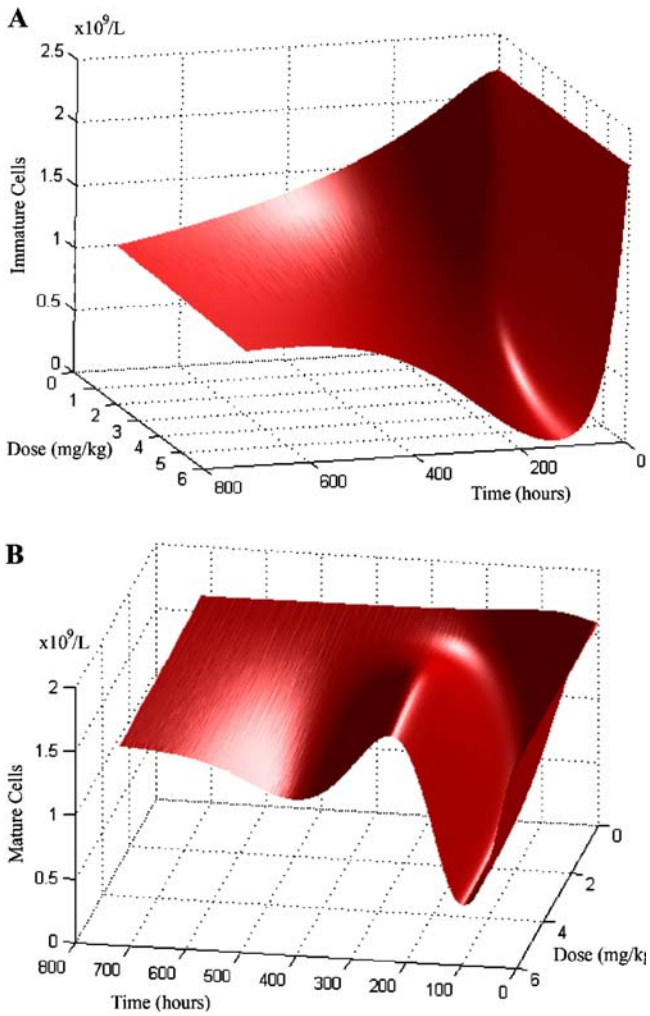

Fig. 5. Simulated time profiles for immature (**A**) and mature (**B**) B-cells as a function of the intra-peritoneal dose of TPT given as a single dose.

lower doses (1.5–2 mg/kg) than for higher doses (>3.5 mg/kg). This phenomenon is explained by the presence of a delay in the non-linear feedback effect for the mature subset. In response to the decrease in that cell subset, the feedback starts to play a role in order to recover the corresponding basal value as soon as possible. However, due to the characteristics of this feedback (not linear and delayed in time), its effect is not linear with respect to the dose. Unfortunately, we have no additional experimental data to support such behaviour detected by computer simulations.

Fig. 7 shows that the dose-related increase in toxicity (expressed as a percentage decrease with respect to baseline) is steeper for progenitor cells (panel A) compared to immature (panel B) and mature B-cells (panel C). Steepness between immature and mature B-cells is similar; however, our model predicts a plateau of 70% maximal toxicity for mature and almost complete depletion of immature (and progenitor) cells. Fig. 7 (panel D) shows the maximal fold change in $k_{Pool} \times Delayed_3$ *vs.* dose relationship. This plot suggests that there is a load capacity; however, those simulation results have to be interpreted with caution, since doses greater than 6 mg/kg were not tested experimentally in the current study.

DISCUSSION

In the field of cancer research, PK/PD models have been developed in different areas ranging from chemotherapy mechanism of action to side effect prediction (27–29). The majority of these models have been focused on the characterization of the time course of absolute neutrophil and leukocyte counts caused by chemotherapy, and very few pay attention to the specific effect over lymphoid lineage cells (4,5).

It is tempting to speculate that if one mechanism of action of chemotherapy includes immunomodulation, a better response to cytotoxic drugs could be obtained, minimizing the harm impinged over antibody-producing B-cells. Therefore, a measure of lymphoid toxicity could be used as a guide to develop more effective dose regimens, incorporating pharmacodynamic data to the predictions.

TPT induced a pronounced decrease in B-lymphocyte subsets, including mature and immature cells. Evidence from experimental data indicates that the dynamics of immature and mature cells severely differ and, thus, cannot be assumed that the latter is just a delayed dynamic of the former. Maybe, the physiological reason for rapidly replenishing the mature B is because this cell population is the principal factory of antibodies, and a priority for the immune system is to maintain antibody levels as normal as possible (30).

In this work, mature circulating B-cells recover baseline values earlier than immature B-cells. To explain this phenomenon, it is necessary to have a source of mature B-cells with self-replenishing capabilities. In the model, the inclusion of the extra depot or pool in the mechanism corresponding to mature cells was based on the results shown by Dammers *et al.* (31), where rats treated with different antitumoral drugs seemed to have relatively unaffected mature B-cell levels, especially the recirculating B-cells, which are predominantly located in lymphoid follicles. In fact, it has been reported that only a minor percentage of the total lymphocytes in the body resides in the blood (32). Moreover, it has been suggested that control mechanisms for immature and mature B-cells operate differently and also both populations differ in the

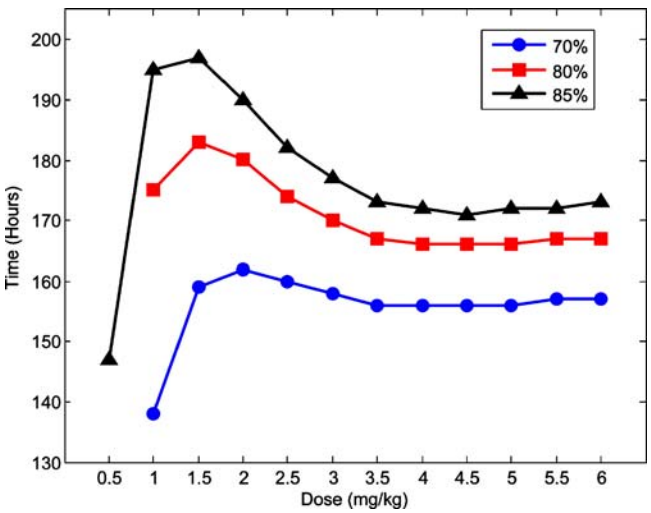

Fig. 6. Recovery time of mature cells to reach different degree the 70% (*blue, circles*), 80% (*red, squares*) and 85% (*black, triangles*) of the basal value depending on the TPT dosage.

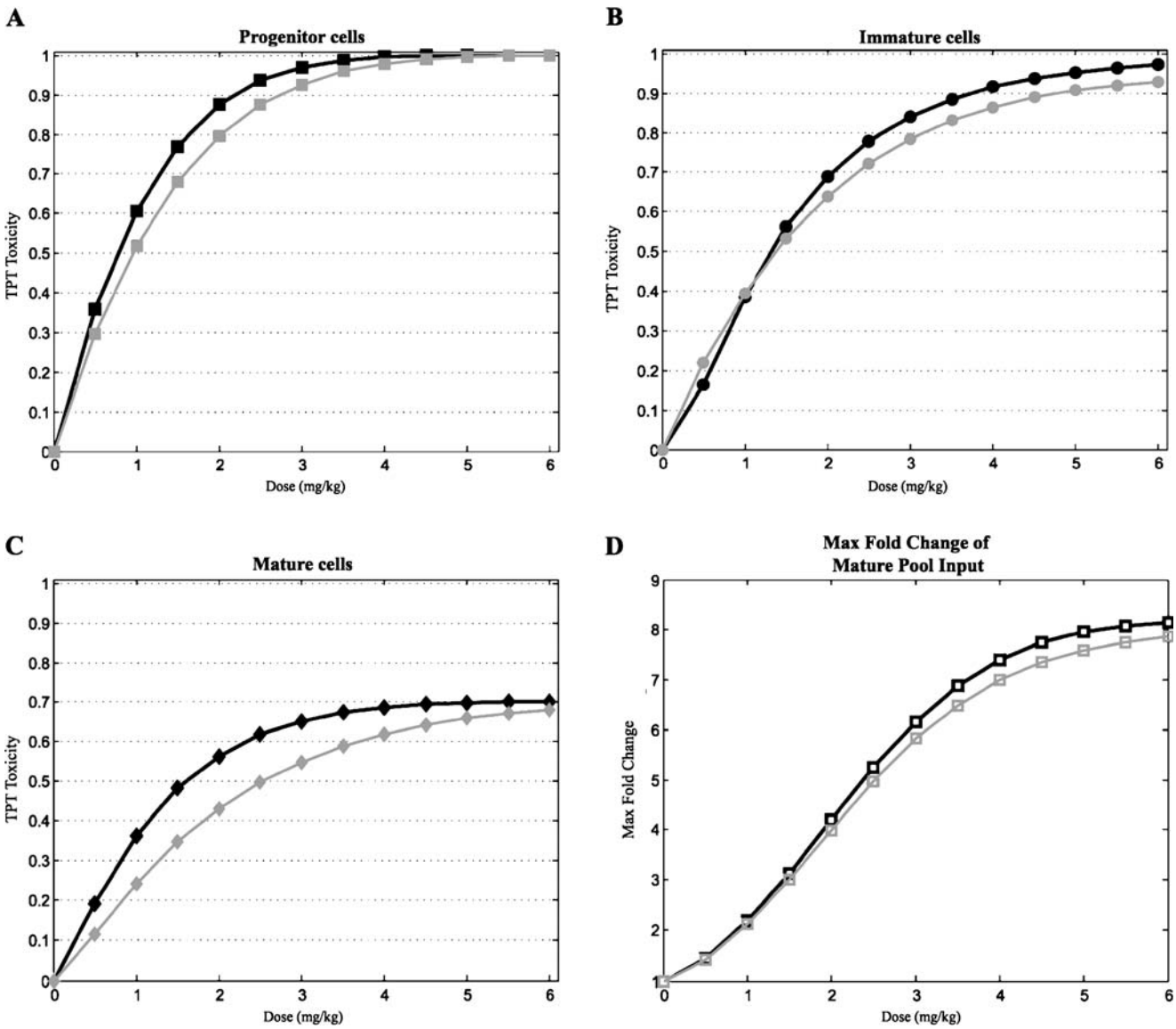

Fig. 7. Simulated maximum percentage of toxicity (expressed as a percentage decrease with respect to baseline) in (A) progenitor population (*square*), (B) immature cells (*circle*) and (C) mature cells (*rhombus*) as a function of the intra-peritoneal dose of TPT administrated following schedule A, single dose (*black*) or schedule B, five consecutive daily doses (*grey*). Maximal fold change in $k_{Pool} \times Delayed_3$ (mature pool input) (D).

sensitivity to drug effects. Immature B-cells depend completely on the continuous production of progenitor cells in the bone marrow, while mature B-cells' peripheral pool homeostasis relies on the growth factors and cytokines at disposal, requiring a small amount supply of newly formed cells (33). Those results are also supported by the current study, where the model developed does not contain a feedback loop between mature and progenitor cells, used previously by Friberg *et al.* (4), because the homeostatic regulation of B-cell compartments has been shown to be independent. Nevertheless, this feedback is appropriated to describe the time profiles of neutrophils in blood. In fact, Segura *et al.* (18) showed the useful application of this mechanism for several blood cells' populations, including total lymphocytes. However, when an intermediate population is measured, such mechanism was not able to describe the experimental data. This observation allowed for including previous feedback in the main organ affected (stem cell compartment) cytostatic agents, such as TPT, acting during the S-phase of the cell-cycle, cells in bone marrow, which divide rapidly, would be mainly affected.

Despite its descriptive capability, the model failed to account for the oscillatory behavior that was observed in the control groups during the first 2–3 days of the study (see upper panels in Fig. 4). Explanations for such phenomena together with the slight continuous decrease of the immature cells in the untreated animals remain unclear, although several explanations could be considered. For example, tumor inoculation process is able to unleash an inflammatory response impinging on immune function. In particular, tumors produce immune suppressor signals that can account for the observed profile of immature cells (34). On the other hand, physical stress by the animal handling could be another of the reasons (32).

Nevertheless, those two unexplained phenomena do not jeopardize the complex behavior of the B-cells' system registered in the treated groups with TPT, accomplished by a very good performance of the developed model.

Another limitation of our study is that the available data were not enough to get any insight into the dynamics of the process that continuously and independently of the immature cells supplies mature B-cells into the bloodstream. This trafficking process was just simply characterized by the zero-order rate constant k_{pool}. It is possible that after prolonged chemotherapy treatments that mechanism becomes less efficient.

Therefore, the model selected did not take into account the trafficking process that has been modelled several times in animals and humans in the past, mostly after corticoids administration. However, different models were explored in an attempt to evaluate the well-known cell trafficking mechanisms. When a peripheral compartment with first-order rate constants k_{in} and k_{out} replacing the zero-order process k_{pool} was incorporated to the model (32), and the delay and feedback processes were affecting k_{in}, the value of AIC was almost 100 points higher (with one extra parameter in the model) than the selected model, indicating clearly that the new model performed worse (model A in Supplementary Material).

When a renewal process of the peripheral compartment (model B in Supplementary Material) was included in the previous model (35), the value of AIC was almost identical (with two extra model parameters) to the one obtained from the selected model.

However, in this case, the baseline value of B-cells in the peripheral compartment was fixed to 45×10^9cells/L. That value was based on the information provided in literature (36), where it could be extracted as the ratio between B-cells in spleen and blood, which is 28, approximately. In addition, one parameter (k_{deg}) was very poorly estimated with a coefficient of variation of 1,582%. The estimates obtained for k_{in} and k_{out} were 0.000198 and 0.0057 h^{-1}, respectively. It is difficult to compare those estimates with others reported in the literature because most of those studies were based on the analysis of total lymphocytes (or T-cells) in blood without discriminating as in our case between different subtypes and subpopulations (32).

In general, immature cells represent less than half of blood B-lymphocytes; however, in immunocompetent rats, such as BDIX rats, the ratio between immature and mature cells was significantly increased (33), an observation that is supported by the estimates of the baseline values of immature and mature cells found in the current study (2.21 *vs*. 1.50×10^9 cells, respectively). The estimate of k_{circ} corresponds to a half-life of 14.1 h, which is in the range of the 26 h value reported previously in the literature for healthy rats (37).

Stochastic differential equations have been used in the development of complex pharmacokinetic/pharmacodynamic models (38,39). Here, we have described simultaneously two variables involving several feedback mechanisms using a less sophisticated, but very effective, hybrid approach based on a combination of qualitative (SD dynamics) and quantitative techniques (parameter estimation). The advantage of this approach was that SD, allowed to accurately propose the structure of the model, reproduced qualitatively the most reliable dynamics of the experimental data.

To summarize the results from the current work, the model developed is the first to elucidate the *in vivo* role on B-lymphocytes subpopulations. The combined measure of mature and immature B-cells is also a unique feature of this study. The major contribution of the model is its new structure and the dynamical consequences, demonstrating an independent behavior between mature and immature B-cells during recovery. In addition, the selected model was further elaborated with the addition of results from the literature to describe the cell-trafficking processes between blood and lymphoid tissues. The proposed models could represent a good basis for the optimization of cytotoxic drugs oriented to attain a maximum antitumor efficacy while minimizing hematological toxicity.

REFERENCES

1. Crawford J, Dale DC, Lyman GH. Chemotherapy-induced neutropenia: risks, consequences, and new directions for its management. Cancer. 2004;100:228–37.
2. Sung L, Nathan PC, Alibhai SM, Tomlinson GA, Beyene J. Meta-analysis: effect of prophylactic hematopoietic colony-stimulating factors on mortality and outcomes of infection. Ann Intern Med. 2007;147:400–11.
3. Rajman I. PK/PD modelling and simulations: utility in drug development. Drug Discov Today. 2008;13:341–6.
4. Friberg LE, Henningsson A, Maas H, Nguyen L, Karlsson MO. Model of chemotherapy-induced myelosuppression with parameter consistency across drugs. J Clin Oncol. 2002;20:4713–21.
5. Friberg LE, Karlsson MO. Mechanistic models for myelosuppression. Invest New Drugs. 2003;21:183–94.
6. Leger F, Loos WJ, Bugat R, Mathijssen RH, Goffinet M, Verweij J, *et al.* Mechanism-based models for topotecan-induced neutropenia. Clin Pharmacol Ther. 2004;76:567–78.
7. Latz JE, Rusthoven JJ, Karlsson MO, Ghosh A, Johnson RD. Clinical application of a semimechanistic-physiologic population PK/PD model for neutropenia following pemetrexed therapy. Cancer Chemother Pharmacol. 2006;57:427–35.
8. Troconiz IF, Garrido MJ, Segura C, Cendrós JM, Principe P, Peraire C, *et al.* Phase I dose-finding study and a pharmacokinetic/pharmacodynamic analysis of the neutropenic response of intravenous diflomotecan in patients with advanced malignant tumours. Cancer Chemother Pharmacol. 2006;57:727–35.
9. Fetterly GJ, Grasela TH, Sherman JW, Dul JL, Grahn A, Lecomte D, *et al.* Pharmacokinetic/pharmacodynamic modeling and simulation of neutropenia during phase I development of liposome-entrapped paclitaxel. Clin Cancer Res. 2008;14:5856–63.
10. Ostby I, Kvalheim G, Rusten LS, Grottum P. Mathematical modeling of granulocyte reconstitution after high-dose chemotherapy with stem cell support: effect of post-transplant G-CSF treatment. J Theor Biol. 2004;231:69–83.
11. Scholz M, Engel C, Loeffler M. Model-based design of chemotherapeutic regimens that account for heterogeneity in leucopoenia. Br J Haematol. 2006;132:723–35.
12. Gaudin E, Rosado M, Agenes F, McLean A, Freitas AA. B-cell homeostasis, competition, resources, and positive selection by self-antigens. Immunol Rev. 2004;197:102–15.
13. Herzog S, Reth M, Jumaa H. Regulation of B-cell proliferation and differentiation by pre-B-cell receptor signalling. Nat Rev Immunol. 2009;9:195–205.
14. Kunkel EJ, Butcher EC. Plasma-cell homing. Nat Rev Immunol. 2003;3:822–9.
15. Casares N, Pequignot MO, Tesniere A, Ghiringhelli F, Roux S, Chaput N, *et al.* Caspase-dependent immunogenicity of doxorubicin-induced tumor cell death. J Exp Med. 2005;202:1691–701.
16. Zitvogel L, Apetoh L, Ghiringhelli F, Kroemer G. Immunological aspects of cancer chemotherapy. Nat Rev Immunol. 2008;8:59–73.

17. Takata T, Suzumiya J, Ishikawa T, Takamatsu Y, Ikematsu H, Tamura K. Attenuated antibody reaction for the primary antigen but not for the recall antigen of influenza vaccination in patients with non-Hodgkin B-cell lymphoma after the administration of rituximab-CHOP. J Clin Exp Hematop. 2009;49:9–13.
18. Segura C, Bandres E, Troconiz IF, Garcia-Foncillas J, Sayar O, Dios-Vieitez C, *et al.* Hematological response of topotecan in tumor-bearing rats: modeling of the time course of different cellular populations. Pharm Res. 2004;21:567–73.
19. Morrisand DL, Komocsar WJ. Immunophenotyping analysis of peripheral blood, splenic, and thymic lymphocytes in male and female rats. J Pharmacol Toxicol Methods. 1997;37:37–46.
20. Crawfordand JM, Goldschneider I. THY1 antigen and B lymphocyte differentiation in the rat. J Immunol. 1980;124:969–76.
21. Beal S, Sheiner L, AJ B. NONMEM user's guide. Ellicot: Icon Development Solutions; 2006.
22. Ludden TM, Beal SL, Sheiner LB. Comparison of the Akaike Information Criterion, the Schwarz criterion and the F test as guides to model selection. J Pharmacokinet Biopharm. 1994;22:431–45.
23. Karlsson M, Holford NH. A tutorial on visual predictive checks, PAGE 17 Abstr 1434 (2008) www.page-meeting.org/?abstract=1434.
24. Mackay F, Schneider P. Cracking the BAFF code. Nat Rev Immunol. 2009;9:491–502.
25. Agenes F, Rosado MM, Freitas AA. Independent homeostatic regulation of B cell compartments. Eur J Immunol. 1997;27:1801–7.
26. Karlsson MO, Savic RM. Diagnosing model diagnostics. Clin Pharmacol Ther. 2007;82:17–20.
27. Bueno L, de Alwis DP, Pitou C, Yingling J, Lahn M, Glatt S, et al. Semi-mechanistic modelling of the tumour growth inhibitory effects of LY2157299, a new type I receptor TGF-beta kinase antagonist, in mice. Eur J Cancer. 2008;44:142–50.
28. Woo S, Krzyzanski W, Jusko WJ. Pharmacodynamic model for chemotherapy-induced anemia in rats. Cancer Chemother Pharmacol. 2008;62:123–33.
29. Panetta JC, Schaiquevich P, Santana VM, Stewart CF. Using pharmacokinetic and pharmacodynamic modeling and simulation to evaluate importance of schedule in topotecan therapy for pediatric neuroblastoma. Clin Cancer Res. 2008;14:318–25.
30. Cancro MP. Peripheral B-cell maturation: the intersection of selection and homeostasis. Immunol Rev. 2004;197:89–101.
31. Dammers PM, de Boer NK, Deenen GJ, Nieuwenhuis P, Kroese FG. The origin of marginal zone B cells in the rat. Eur J Immunol. 1999;29:1522–31.
32. Yao Z, DuBois DC, Almon RR, Jusko WJ. Pharmacokinetic/pharmacodynamic modeling of corticosterone suppression and lymphocytopenia by methylprednisolone in rats. J Pharm Sci. 2008;97:2820–32.
33. Milicevic NM, Nohroudi K, Milicevic Z, Hedrich HJ, Westermann J. T cells are required for the peripheral phase of B-cell maturation. Immunology. 2005;116:308–17.
34. Mellor AL, Munn DH. Creating immune privilege: active local suppression that benefits friends, but protects foes. Nat Rev Immunol. 2008;8:74–80.
35. Krzyzanski W, Jusko WJ. Indirect pharmacodynamic models for responses with multicompartmental distribution or polyexponential disposition. J Pharmacokinet Pharmacodyn. 2001;28:57–78.
36. Zandvoort A, Lodewijk ME, Klok PA, Dammers PM, Kroese FG, Timens W. Slow recovery of follicular B cells and marginal zone B cells after chemotherapy: implications for humoral immunity. Clin Exp Immunol. 2001;124:172–9.
37. Westwemann J, Puskas Z, Pabbst R. Blood transit and recirculation kinetics of lymphocyte subsets in normal rats. Scand J Immunol. 1988;28:203–10.
38. Tornøe CW, Agersø H, Senderovitz T, Nielsen HA, Madsen H, Karlsson MO, *et al.* Population pharmacokinetic/pharmacodynamic (PK/PD) modelling of the hypothalamic-pituitary-gonadal axis following treatment with GnRH analogues. Br J Clin Pharmacol. 2007;63:648–64.
39. Overgaard RV, Holford N, Rytved KA, Madsen H. PKPD model of interleukin-21 effects on thermoregulation in monkeys–application and evaluation of stochastic differential equations. Pharm Res. 2007;24:298–309.